Cooperative Control of UAVs for Localization of Intermittently Emitting Mobile Targets

Daniel J. Pack, *Senior Member, IEEE*, Pedro DeLima,
Gregory J. Toussaint, *Senior Member, IEEE*, and George York

***Abstract*—Compared with a single platform, cooperative autonomous unmanned aerial vehicles (UAVs) offer efficiency and robustness in performing complex tasks. Focusing on ground mobile targets that intermittently emit radio frequency signals, this paper presents a decentralized control architecture for multiple UAVs, equipped only with rudimentary sensors, to search, detect, and locate targets over large areas. The proposed architecture has in its core a decision logic which governs the state of operation for each UAV based on sensor readings and communicated data. To support the findings, extensive simulation results are presented, focusing primarily on two success measures that the UAVs seek to minimize: overall time to search for a group of targets and the final target localization error achieved. The results of the simulations have provided support for hardware flight tests.**

***Index Terms*—Cooperative, distributed control, localization, unmanned aerial vehicles (UAVs).**

I. Introduction

STARTING from early remotely piloted reconnaissance missions in 1960s, the military role of unmanned aerial vehicles (UAVs) has grown both in relevance and scope. Currently, UAVs are used in border patrol, police task forces, weather data collection, search and rescue missions, and a number of military operations involving intelligence gathering, surveillance, and reconnaissance.

Traditionally, researchers have strived to develop a single sophisticated UAV to perform complex tasks. In [1], control strategies were developed for a single UAV to provide sensory data, as well as communication between and coordination of ground units. The efficiency of different trajectory planning algorithms was compared in [2] for a single UAV approaching multiple targets in a convex unobstructed space. Moreover, in [3], multiple images from a single UAV were used to reconstruct 3-D images of buildings.

Although many single UAV applications can be carried out successfully through manual operation, only autonomous systems can provide solutions to some applications, such as extensive continuous reconnaissance operations lasting weeks or months [4]. Moreover, several recent independent results in target search [5], target observation [6], cooperative transportation [7], and path coordination [8] have made clear that more complex applications that were beyond the reach of single units became achievable using multiple systems working cooperatively. The emergence of multiple-UAV solutions, such as the UAV platforms in which we have conducted flight experiments, shown in Fig. 1, led to an even greater need for flight and decision automation, due to the long recognized limitations of manual operation of multiple multitasking UAVs [9].

Fig. 1. Autonomous UAV platform outfitted with RF and camera sensors.

Considerable work has been performed in the generation of distributed strategies for searching for targets in vast areas [5], [10]. However, to our best knowledge, none has considered intermittently emitting radio frequency (RF) targets. In this paper, we propose a novel cooperative UAV control architecture to search, detect, and localize RF mobile ground targets. Examples of RF ground mobile emitters in real-world applications include tracking of ground personnel based on sporadic communication and the localization of Integrated Air Defense System units. At the core of the proposed architecture is a distributed decision logic that each UAV applies to independently determine its operating state in response to environmental information gathered from its own sensors and from communicating with neighboring UAVs.

Within the scope of our solution, two key issues can be identified. First, an effective search strategy must be decentralized in execution and cooperative in nature at the same time [11]. In [12], ground mobile platforms search an area using a probabilistic approach that combines the cost of reaching a target with its impact on the group's coverage of a search area. In our approach, each UAV also takes into consideration the desire to remain distant from other UAVs to maximize coverage and stay within the boundaries of a search area. In this paper, we isolate the impact of each of these factors on the overall effectiveness of the proposed search strategy in a sequence of simulations, in turn demonstrating their contribution and relevance.

Manuscript received September 19, 2006; revised May 25, 2007, January 14, 2008, May 29, 2008, and September 25, 2008. First published March 24, 2009; current version published July 17, 2009. This paper was recommended by Associate Editor M. Dorigo.

The authors are with the Department of Electrical and Computer Engineering, U.S. Air Force Academy, CO 80840 USA (e-mail: daniel.pack@usafa.edu; pedro.lima@usafa.edu; gregory.toussaint@usafa.edu; george.york@usafa.edu).

Color versions of one or more of the figures in this paper are available online at http://ieeexplore.ieee.org.

Digital Object Identifier 10.1109/TSMCB.2008.2010865

Report Documentation Page

Form Approved
OMB No. 0704-0188

1. REPORT DATE	2. REPORT TYPE	3. DATES COVERED
2009		**00-00-2009 to 00-00-2009**

4. TITLE AND SUBTITLE	5a. CONTRACT NUMBER
Cooperative Control of UAVs for Localization of Intermittently Emitting Mobile Targets	5b. GRANT NUMBER
	5c. PROGRAM ELEMENT NUMBER
6. AUTHOR(S)	5d. PROJECT NUMBER
	5e. TASK NUMBER
	5f. WORK UNIT NUMBER
7. PERFORMING ORGANIZATION NAME(S) AND ADDRESS(ES) **Department of Electrical and Computer Engineering,U.S. Air Force Academy,CO,80840**	8. PERFORMING ORGANIZATION REPORT NUMBER
9. SPONSORING/MONITORING AGENCY NAME(S) AND ADDRESS(ES)	10. SPONSOR/MONITOR'S ACRONYM(S)
	11. SPONSOR/MONITOR'S REPORT NUMBER(S)

12. DISTRIBUTION/AVAILABILITY STATEMENT
Approved for public release; distribution unlimited

13. SUPPLEMENTARY NOTES
Government or Federal Purpose Rights License

14. ABSTRACT

15. SUBJECT TERMS

16. SECURITY CLASSIFICATION OF:			17. LIMITATION OF ABSTRACT	18. NUMBER OF PAGES	19a. NAME OF RESPONSIBLE PERSON
a. REPORT	b. ABSTRACT	c. THIS PAGE			
unclassified	**unclassified**	**unclassified**	**Same as Report (SAR)**	**12**	

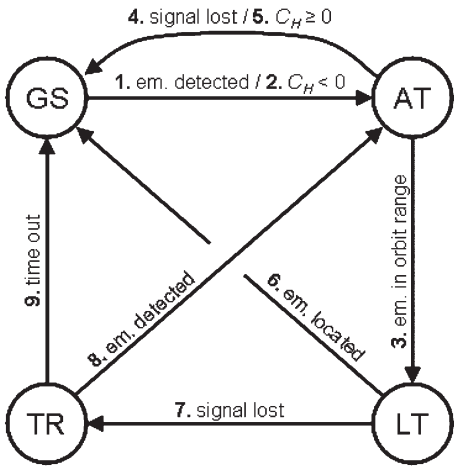

Fig. 2. Decision state machine for UAV state selection. The numbered events that trigger each particular directional connector are listed in Table I.

The second key issue rests on the target localization technique used. Even with the provision in the proposed architecture to efficiently reacquire a target when the target stops emitting before being fully localized, the localization accuracy and speed have a direct impact on the effectiveness of the overall search and localization task. We explore the benefits of three different techniques for target localization in a multisensor environment using only an angle-of-arrival (AOA) sensor information. Namely, we investigate the performance of triangulation [13], angle-rate [14], and Kalman filtering [15], [16] techniques.

This paper is organized as follows. Section II details the proposed cooperative distributed UAV control architecture, followed by a description of two key issues: decentralized search and target localization. Section III explores the proposed decentralized global search (GS) methodology. Section IV describes the three techniques we used to localize targets using only AOA data from multiple mobile sensors. Section V presents encompassing simulation results that demonstrate the capability of the proposed architecture to search for and localize intermittently emitting mobile targets. We conclude this paper with a summary in Section VI.

II. Cooperative UAV Control Architecture

We have developed a behavior-based distributed control architecture [17], [18] to maximize the capabilities of multiple UAVs to search for, detect, and localize multiple RF emitting targets. The distributed control architecture dictates that each UAV governs its own operation through a decision state machine composed of four states: GS, approach target (AT), locate target (LT), and target reacquisition (TR). Fig. 2 shows the state machine, where the decision to change from one state to another is represented by arrows triggered by the different events summarized in Table I. It is important to note that only a limited amount of communication between UAVs and the base station is required. When in flight, each UAV broadcasts to the group only its position, its heading, a sensed/estimated target position (AT and LT only), and a help request when necessary. Completing the list of all communications exchanged in flight, the base station broadcasts to all UAVs the estimated number of targets still left undetected in the field, whenever this estimate changes. Although discussing the implemented communication protocol [19] in detail goes beyond the scope of this paper, the small information exchange demand allows the assumption of ideal communication between all members.

TABLE I
List of Events That Trigger Decisions to Change States in the Decision State Machine of Each UAV

#	From	Event	To
1	GS	New emitter detected by UAV's sensor.	AT
2	GS	Decision to cooperate with an ongoing localization effort ($C_H < 0$). See Section II.B for C_H	AT
3	AT	UAV arrives in orbit range from emitter's estimated position.	LT
4	AT	Emitter stops transmitting.	GS
5	AT	Decision to cooperate with an ongoing localization effort no longer supported ($C_H \geq 0$).	GS
6	LT	Emitter successfully located.	GS
7	LT	Emitter stops transmitting.	TR
8	TR	Emitter detected by UAV's sensor.	AT
9	TR	Maximum time for TR reached.	GS

A. Global Search

While in the GS state, a UAV flies to detect targets with an omnidirectional RF sensor. However, since the targets are mobile and intermittently emitting signals, simply covering the entire search area once is not sufficient to guarantee target detection. Instead, we use the concept of dynamic coverage in a manner similar to the one applied in [20] to measure the frequency in which different sections of a search area are scanned. More specifically, in order to maximize target detection, a team of UAVs involved in a joint search effort seeks to increase the average visiting frequency of all sections of the search area in a homogeneous manner (i.e., revisit every section of the search area with the same frequency).

In addition to these two team goals, each UAV must also achieve two individual search goals. First, in order to quickly respond to changes in the number of UAVs involved in the search effort, and to make it harder for targets to actively avoid detection, a UAV must not make use of predetermined search patterns such as lawn-mower serpentine patterns [21]. Second, due to the limited energy supplies intrinsic to UAV applications, it is also important that the search pattern generated by a UAV minimizes the intensity of the UAV's maneuvers. Although always in play, this factor is of particular interest when UAVs search an area since, in practice, lower energy consumption allows for longer uninterrupted search times.

B. Approach Target

In the AT state, a UAV seeks to move into an orbit around a detected emitter. We define the orbit as all points with a user-specified desired radial distance from the estimated emitter location around which UAVs can fly safely. A UAV may change its operational state from GS to AT if it detects an emitter currently not detected by any other UAVs (Event 1 in Table I) or if it decides to stop contributing to the GS and lend assistance to an ongoing target localization effort (Event 2). A UAV decides

to help a localization effort being conducted by other UAV(s) when the help cost C_H, given in (1), becomes negative

$$C_H = w_1 D_e - w_2(c_{\max} - c) + w_3(f_{\max} - f) \quad (1)$$

where D_e stands for the normalized estimated Euclidean distance from the current UAV location to the emitter. The desired maximum number of UAVs to cooperatively locate a target is denoted by $c_{\max}$, while c stands for the number of UAVs already committed to a particular emitter localization effort. In the third term, $f_{\max}$ stands for the total estimated number of emitters in the search space, and f stands for the number of emitters that have already been detected or located. If $f_{\max}$ is not known with precision, an expected number can be used. In most cases, it is advised to overestimate the total number of emitters to ensure that not too many UAVs will stop contributing to the GS effort before all emitters are found. Finally, the w_i's are weights an operator can assign to influence the behavior of the UAVs, allowing for problem-specific solutions. Note that this cost function is a result of the inherent tradeoff between remaining in GS and therefore increasing the collective search capability, against committing to increase the speed and accuracy of localizing a single emitter.

In the same manner as a UAV operating in GS that switches its state to AT when C_H becomes negative, a UAV may return to the GS state if the help cost becomes positive due to the actions of other UAVs (Event 5). A UAV also returns to the GS state if the target of interest stops emitting (Event 4) while the UAV is approaching the target. Provided that the cost remains negative, the UAV switches its operating state to the LT state when it reaches the target's orbit (based on its current estimated position; Event 3).

C. Locate Target

A UAV operating in the LT state orbits around the estimated emitter position, while taking new sensor readings. The current implementation allows up to three UAVs to join in the effort to locate an emitter, providing simultaneous AOA sensor readings from different viewpoints. Techniques such as triangulation, an angle-rate algorithm, and Kalman filtering are used to increase the accuracy of the target localization process by combining information provided by different UAVs and sensor data collected at different moments in time. Once a target is accurately located, all UAVs orbiting the target return to the GS state (Event 6). Otherwise, if a target stops transmitting, all UAVs orbiting the target switch to the fourth state, which is TR (Event 7).

D. Target Reacquisition

TR is a state that is only reached by orbiting UAVs operating in LT when their target emitter stops transmitting before the emitter is accurately located. UAVs operate in one of two phases within the TR state.

During the initial phase, UAVs continue to orbit around the last estimated emitter position with an increasing orbit radius over time. The resulting flying path is a growing spiral with a rate of expansion dictated by the estimated emitter's maximum speed and the last two readings of the estimated emitter location. Once a predefined time period has passed without a reacquisition of the target, UAVs operating in TR enter into the second phase.

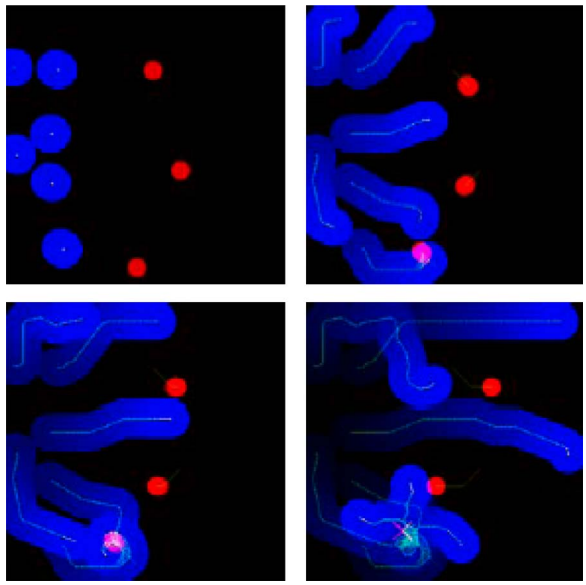

Fig. 3. Simulation snapshots. The top-left frame shows the initial locations of (large circles) six UAVs as they start under the GS state to search for (small circles) three targets. The top-right frame shows a target (at the bottom of the frame) being detected by a UAV, which assumes the AT state and transmits to nearby UAVs its discovery. Upon receiving the target discovery information, the nearby UAVs determine whether to help localize the target. The frame shows that two of the nearby UAVs have decided to join the efforts. In the bottom-left frame, two UAVs are now close enough to the target to assume the LT state and start orbiting it. The bottom-right frame shows that the bottom target has been accurately located, and the three involved UAVs return to the GS state.

In the second phase, UAVs perform a local search similar to the GS, except in a limited area around the emitter's last estimated position. If an emitter is still not detected after a user defined maximum amount of time, the associated UAVs discontinue the local search and switch to operate in the GS state (Event 9). A TR effort is successful if, during one of the two phases, an emitter is detected. In this circumstance, the UAVs switch back to the AT state (Event 8).

A simulation output illustrating the typical UAV states and cooperative synergistic behaviors can be seen in Fig. 3. In this simulation, we assume that each UAV possesses a Global Positioning System sensor to determine its location, which is shared with other nearby UAVs, and only a rudimentary AOA sensor for sensing target locations. The RF signal emitted by the target is assumed to be omnidirectional, and the actual emission is intermittent, with random on and off times. The same simulator is used in the remainder of this paper with slight variations to size of the search areas and UAV characteristics in order to focus on matters relevant to each section individually. Further details of its characteristics are given in the appropriated sections.

III. Cooperative Search

As a distributed control system, cooperative search patterns must be generated by the actions taken by each UAV individually based only on locally available information. Therefore, in our proposed search algorithm, each UAV seeks to achieve both

team and individual goals by evaluating different maneuvering options under the search cost C_S shown in the following, which combines the group's dispersion pattern, the search history of the UAV's immediate neighborhood, and the fuel consumption necessary for each particular maneuver:

$$C_S = H_{x,y}\left(\frac{1}{\sum(D_i)} + \frac{1}{\sum(D_j)}\right)|\Delta\phi_{\mathrm{UAV}}| \tag{2}$$

where $H_{x,y}$ corresponds to a numerical value representing the explored history of a location indexed by x, over an east–west axis, and y, over a north–south axis. The history matrix H (i.e., a history map) is generated and maintained by each UAV by assigning to each cell, mapped to a small subregion of the search area, the maximum value of one when a team member scans it with its sensor(s) and constantly decrementing the entries in all cells by a small value over time in order to represent the deterioration of information with the passage of time. The sum of the distances from a UAV to its peers and the sum of the distances between a UAV and the search area boundaries are represented by $\sum(D_i)$ and $\sum(D_j)$, respectively. Finally, the change in the heading angle required to reach a particular location is represented by $\Delta\phi_{\mathrm{UAV}}$. By evaluating C_S in different locations around its current position, a UAV continuously flies in the direction of the location with the minimum search cost. Note that, although $\sum(D_i)$ adds the intentionality of dispersion to the cost function C_S, it does not guarantee collision avoidance. In practice, this issue is dealt with by having the cooperating UAVs operate at different altitudes.

The proposed search strategy based on the evaluation of C_S has as it primary goals as follows: 1) to increase the rate at which it revisits each area; 2) to reduce the variability of the visitation frequency across the entire search area; and 3) to minimize energy consumption by reducing the number and intensity of maneuvers performed by the UAVs. To demonstrate the role of the four components that make up the proposed C_S, we now present a number of cost functions composed of combining the four components incrementally. In Section V, we show the statistically supported simulation results.

The first most basic component of the search cost reflects a UAV's intention to simply remain within the search area. The first search cost function C_S^1 only assigns nonzero costs to areas outside the search area, making a UAV fly in a straight trajectory, maneuvering only when necessary to remain within the search area. Since this reaction is the minimum necessary for a team to achieve measurable values for the three goals, the results of the simulations based on C_S^1 are treated as the baseline for comparison with the other costs in Section V.

In the second search cost function, we add the intention of a UAV to navigate to an area that has not been visited for the longest time, as stored in the search history matrix H. This intention, coupled with higher costs associated with areas closer to search boundaries, forms C_S^2, as shown in (3). For the third cost function, we add the concept of cooperative search area coverage to the search cost by increasing the cost of destinations closer to other cooperating UAVs. As shown in (4), this is done in C_S^3 through the insertion of the term related to $\sum(D_i)$, where D_i denotes the distance from a UAV to its ith neighbor. Finally, C_S^4 described in (5) incorporates all proposed components, being equal to the initial C_S

$$C_S^2 = H_{x,y}\left(\frac{1}{\sum(D_j)}\right) \tag{3}$$

$$C_S^3 = H_{x,y}\left(\frac{1}{\sum(D_i)} + \frac{1}{\sum(D_j)}\right) \tag{4}$$

$$C_S^4 = H_{x,y}\left(\frac{1}{\sum(D_i)} + \frac{1}{\sum(D_j)}\right)|\Delta\phi_{\mathrm{UAV}}|. \tag{5}$$

In order to measure the impact of each search cost over the three stated goals, the following metrics were used. To measure the average frequency at which any given point in the search area is visited, the dynamic coverage (dc) of the search area is measured through the following by obtaining the average value of the cells of the history matrix of the search area H:

$$dc = \frac{\sum_x \sum_y H_{x,y}}{N} \tag{6}$$

where N corresponds to the total number of cells in the matrix H.

To measure the variability, or heterogeneity, of the coverage effort, the standard deviation of the cells of the history matrix at a given time σ_H is calculated using (7). Note that, the more uniform the search is, the smaller the standard deviation of the coverage in the history matrix, and therefore, the goal is to design a search strategy that leads to minimum heterogeneity

$$\sigma_H = \sqrt{\frac{\sum_x \sum_y (H_{x,y} - dc)^2}{N}}. \tag{7}$$

Finally, the amount of energy required by a team to search an area is measured by the total amount of turns, in degrees, involved in all maneuvers conducted by the cooperating UAVs while inside the search area (in this manner, eliminating the impact of the maneuvers required simply to remain inside the search area). Section V shows the simulation results.

IV. Cooperative Localization Techniques

In this section, we describe three different cooperative localization techniques that we implemented for the LT state: triangulation, angle-rate algorithm, and Kalman filtering. All three techniques can be used with one or multiple sensor platforms. If only a single mobile platform is used when the triangulation technique is employed, the target must be stationary. For mobile targets, the triangulation of synchronous readings is used only, and therefore, the accuracy of the triangulation technique is limited to the number of sensor platforms and does not improve with time. The angle-rate algorithm is normally limited to locate stationary emitters when a single mobile platform is used, and compared to the triangulation technique, it is capable of achieving better performance in small included angle scenarios. Finally, Kalman filtering techniques are capable of gradually increasing the localization accuracy of stationary and mobile emitters, independent of the number of sensor platforms used. However, Kalman filters require *a priori* knowledge of the emitter's dynamic behavior and the stochastic characteristics of the sensors used.

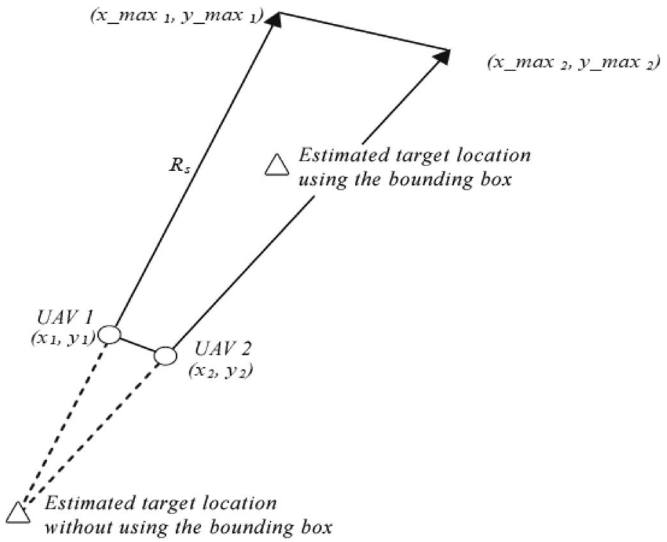

Fig. 4. Approach to avoid poor estimates for the triangulation localization technique. The quadrilateral bounding box is used to filter out poor estimates.

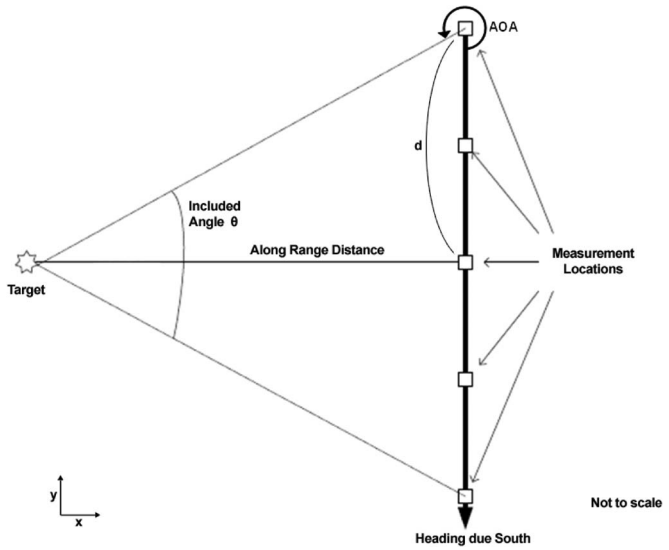

Fig. 5. Basic UAV and target geometry.

A. Triangulation

The directional sensor mounted on each UAV provides an estimated angle ϕ_i to the target with respect to a fixed coordinate frame onboard a UAV, at time k for each estimate i. The UAV position with respect to a world coordinate frame is denote as (x_i, y_i). The distance to a target is unknown but is bounded by the maximum sensor range R_s. Given two UAVs within R_s of the target or one UAV with two estimates close in time, we can triangulate the target location based on the two estimates by simply finding the intersection of the two lines defined by the estimates. When we have three estimates to triangulate (due to three UAVs or one UAV over time), we triangulate between each pair of the three estimates. We then estimate the target location from the centroid of the triangle defined by these three points.

Triangulation is known for producing poor estimates when the two UAVs produce measurements with very similar slopes. Such measurements occur when either two UAVs are flying close to each other or a single UAV takes one sensor reading shortly after another. Due to their sensor error, instead of the triangulation point being near the target, the almost parallel lines can result in an intersection far beyond the range R_s or they can even diverge, resulting in an intersection point in the wrong direction, as shown in Fig. 4. To avoid these extreme cases, we test to see if the triangulation point is inside of a bounding quadrilateral defined by the two UAV locations (x_i, y_i) and the points $(x\_\max_i, y\_\max_i)$ along the angle to the target ϕ_i at the maximum sensor range R_s. If the resulting target estimation lies inside this quadrilateral, the triangulation estimate is accepted. If the estimation lies outside of the quadrilateral, we can instead estimate the location to be the median point between the UAV positions and the other two quadrilateral vertices $(x\_\max_i, y\_\max_i)$.

B. Angle-Rate Algorithm

When the slopes of the measurements of two or more UAVs are similar, sometimes referred as having small included angles between angle measurements or large geographic dilution of precision (GDOP) conditions, the angle-rate algorithm renders improved localization results than the ones obtained using the triangulation technique, as we will show in Section V. The following two factors make large GDOP conditions likely to occur in our problem of interest: 1) Each sensor is mounted on a slowly moving UAV that prevents it from significantly changing its relative position from one sensor measurement to the next and 2) intermittently emitting targets can stop emitting before the cooperating UAVs have time to improve their relative positions.

Recall that, for a rotating object, the tangential velocity is equal to the angular velocity multiplied by the distance to the axis of rotation. We can compute the range to the target once we obtain the angle rate [i.e., $r(d\theta/dt) = (dy/dt)$] if the included angle is small. For a general case, we need to use trigonometrical identities [i.e., $\tan(\theta) = (d/range)$] to compute the range values. For the geometry described in Fig. 5, the emitter's calculated range is one half of the UAV's y-distance traveled (d) divided by the tangent of one half of the included angle (θ). To compute the included angle accurately, we find the *average* AOA, *average* AOA rate, and *average* included AOA that are obtained from the linear least square regression of the measured AOA data. Once we find the average AOA, we compute the average AOA rate and, subsequently, the desired average included AOA to compute the tangent range.

The emitter location's calculated y-value, or cross-range, is the UAV's average y-value added to the emitter's range multiplied by the tangent of the average included AOA [i.e., $\hat{y} + r\tan(\theta)$]. Note that using the *average* AOA obtained via linear regression instead of a tangent regression curve adds a bias to the range estimate. For small included angles where $\tan(\alpha) \approx \alpha$, the bias is negligible.

C. Kalman Filter

Kalman filtering is used as a model-based observer to generate minimum covariance localization estimates based on the sensor measurements of multiple UAVs over time. In order to

apply the Kalman filter, the first step is to model our RF target localization problem with the following difference equation:

$$x[k] = Ax[k-1] + Bu[k] + w[k-1] \tag{8}$$

where $x[k] \in R^4$ denotes the position and velocity of the target at time k, $u[k]$ is the forcing function, and $w[k]$ is the process Gaussian white noise with mean value zero and covariance matrix Q. Matrices A and B relate the previous time state and inputs with the current time state, describing the characteristics of the target's dynamic system. We assume that our sensors can measure only the position of a target as shown as follows:

$$y_i[k] = C_i x[k] + v_i[k]. \tag{9}$$

Matrix C_i denotes the measurement matrix, $y_i[k] \in R^2$ is the position measurement at time k, and v_i represents a Gaussian white measurement noise with zero mean and covariance matrix R_i for the sensor on UAV i. We can model a directional sensor by appropriately selecting the contents of covariance matrix R_i. We also assume that the process and measurement noise are independent of each other.

Given the target and sensor models, the task of target location transforms into a problem of minimizing the corresponding error covariance, where an error denotes the difference between an estimated position and the true target position. For a more formal and complete description of the filter, the reader is directed to [22]. In essence, the optimal filtering algorithm uses the time and measurement update equations to predict and update the error covariance of a target as new sensor measurement is acquired. The localization task then becomes a recursive process to reduce the error covariance.

V. Simulation Results and Analysis

We now present three different simulation results that demonstrate the capability of teams of UAVs to accomplish the entire mission of searching for and localizing intermittently emitting mobile targets over large areas. Section V-A presents the results validating the search strategy presented in Section III, followed by the target localization results using the triangulation, angle-rate, and Kalman filter algorithms illustrated in Section IV. In this section, we also identify preferred regions to use the triangulation and angle-rate algorithms. Section V-C is dedicated to present the overall performance of multiple UAVs searching, detecting, and locating ground targets.

A. Impact of the Components of the Proposed Search Strategy

Results in this section were obtained by simulating a team of four UAVs, randomly initialized inside a 4 km $\times$ 4 km search area operating for 1 h using the C_S^1, C_S^2, C_S^3, and C_S^4 cost function strategies while measuring the following three metrics: 1) dynamic coverage dc; 2) heterogeneity σ_H (i.e., search variability); and 3) the amount of UAV maneuvers. All UAVs were set to a cruise speed of 65 km/h with a maximum allowed turn rate of 2°/s, modeling typical responses of small fixed wing aircraft. Each UAV's model is outfitted with sensors with a radial maximum range of 400 m and a sensing interval of 2 s. To account for the variability of the results, 50 simulation runs were performed for each search cost strategy with the final results listed in Table II. All results were evaluated by pairs against the null hypothesis of equal means $(\alpha = 0.05)$ using the standard t-test when the equal variance hypothesis could not be rejected $(\alpha = 0.1)$ or using the Satterthwaite's approximation to the t-test otherwise.

TABLE II
Simulation Results at the End of 1 H for Search Conducted According to Each C_S Completion Level. Results in Mean (Standard Deviation) Notation

Goals	Dynamic Coverage	heterogeneity	Internal Maneuvers
C_S^1	0.708 (0.028)	0.064 (0.014)	0 (0)
C_S^2	0.774 (0.016)	0.034 (0.004)	6980 (479)
C_S^3	0.784 (0.011)	0.029 (0.003)	6747 (417)
C_S^4	0.778 (0.014)	0.031 (0.004)	3120 (334)

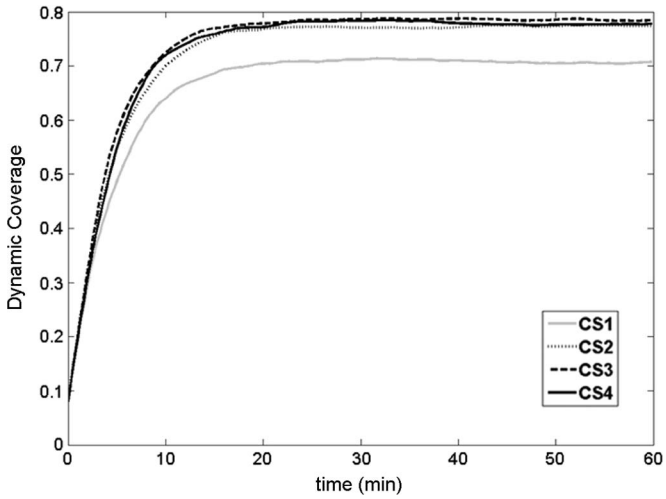

Fig. 6. Average dynamic coverage of teams of four UAVs subject to different levels of completion of the search cost C_S.

The average evolution of the dynamic coverage, which is the first metric used to evaluate the proposed search algorithm, during the 1 h of simulation can be seen in Fig. 6. As expected, search using C_S^2, C_S^3, and C_S^4 performs significantly better than the baseline one using C_S^1. On a closer analysis between the top three performers, the results indicate that the addition of the component that creates a repelling force between team members introduced in C_S^3 outperforms C_S^2 with a comparatively less drastic yet statistically significant $(p < 0.001)$ higher mean at the end of the simulation. On the other hand, the addition of the component that forces UAVs to reduce the intensity of maneuvers in C_S^4 resulted in an inferior average response compared to the one by C_S^3, but still more successful than that of C_S^2. At the end of the simulation, the average dynamic coverage achieved using C_S^4 was significantly smaller $(p = 0.017)$ than that of C_S^3, but did not present a significant difference $(p = 0.116)$ from that of C_S^2.

Fig. 7 shows the results pertaining to the second metric, which is the minimization of the heterogeneity σ_H of the search. Although these are independent measures, the results are similar to the ones for the dynamic coverage, with search using C_S^2, C_S^3, and C_S^4 outperforming the baseline, and the average response of C_S^4 remaining between that of C_S^2 and

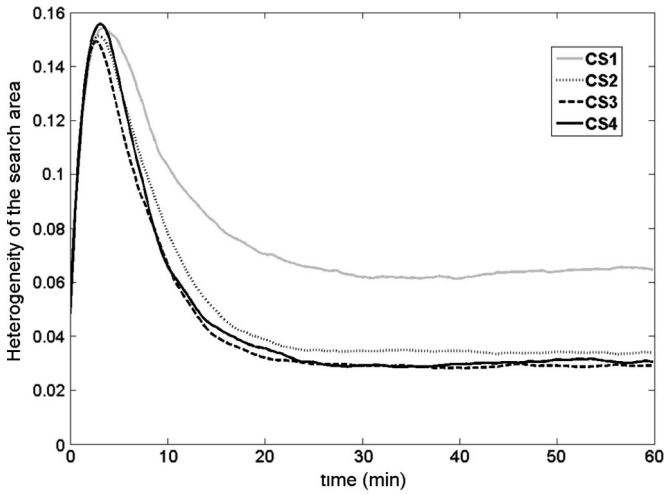

Fig. 7. Heterogeneity levels achieved by teams of four UAVs under different levels of completion of the search cost C_S. Lower levels indicate greater homogeneity of the search effort.

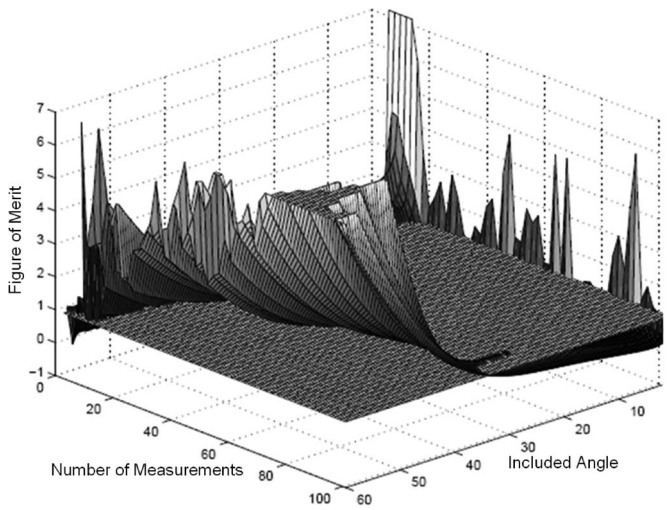

Fig. 8. FOM for included angles from 0° to 60°.

C_S^3 during almost the entire simulation time. On the other hand, all final search costs present significantly different means ($p < 0.001$ for all pairs, except for the comparison of the means of C_S^3 and C_S^4, which presented $p = 0.046$), with the mean value of the heterogeneity obtained by C_S^4 closer to that of C_S^3 than to that of C_S^2.

Finally, the results for the total fuel consumption while within the search area shown in Table II bring four significantly different ($p < 0.001$ for all pairs, except for the comparison of the means of C_S^2 and C_S^3, which presented $p = 0.011$) outcomes. Note that, since the baseline C_S^1, by construction, does not perform maneuvers while within the search area, it represents the minimum fuel consumption for this measure, receiving zero value. It is noteworthy to point out that the improved results achieved by using C_S^3 over C_S^2 on the other two metrics were not reached at the expense of greater fuel consumption, as observed by the small, yet statistically significant, difference between their final compounded maneuvers. More importantly, the results obtained by using C_S^4, which is the complete proposed search cost, show that less than half of the total degrees of maneuvers were performed by the UAVs compared to the ones recorded when C_S^2 or C_S^3 was used. Although the exact relationship between the characteristics of the maneuvers and the ultimate flight autonomy is aircraft dependent, it is possible to state that a drop of such intensity on the UAVs maneuvers has a significant impact on the flight time of a UAV capable of uninterruptedly searching an area for targets.

In summary, the incremental addition of the four basic components has shown that allowing UAVs to make use of the information contained in H has the greatest impact on dynamic coverage and heterogeneity but requires the largest amount of energy to be expended. Adding to the UAVs, the intention to keep distance from other cooperating UAVs, in the manner formulated in the proposed search cost strategy, leads to a smaller, yet significant, improvement on all three metrics, making this an improvement without any detrimental effect. Finally, the completion of the proposed search cost with the inclusion of the intention to reduce the magnitude of the maneuvers of each UAV results in a slight reduction of the dynamic coverage and heterogeneity gains achieved by the addition of the previous factor, which is a comparatively small price to pay for the resulting great drop in energy consumption which, in practice, allows search missions to be carried out for longer periods of time.

B. Target Localization

In this section, we compare target localization results when the triangulation and angle-rate localization techniques are used by multiple UAVs, describing conditions where one technique outperforms the other. Next, we show target localization results when Kalman filtering techniques are used.

1) Triangulation and Angle-Rate Techniques: To compare the triangulation and angle-rate algorithms, we varied the number of measurements and the included angle values. By keeping the noise constant with a covariance of one, we collected the accuracy data as we varied the number of measurements from 3 to 101 and the included angle from 0.5 to 60°.

The along-range error (x-axis in Fig. 5) is the dominant term in the error calculations, since the along-range error corresponds to the semimajor axis of the error probable, and for large GDOP, our error is highly elliptical. When comparing the performance of the two algorithms, we used only the square of the along-range error since the cross-range error (y-axis in Fig. 5) was much smaller in magnitude. The figure of merit (FOM) we used to compare the algorithms' performance is

$$FOM = \frac{\sigma^2_{\text{along-range-angle rate}}}{\sigma^2_{\text{along-range-triangulation}}} \tag{10}$$

where σ represents the standard deviation of the error.

In (10), FOM less than one means the angle-rate algorithm resulted in a smaller average error, while FOM greater than one means the triangulation algorithm resulted in smaller average error.

Fig. 8 shows a 3-D plot of the FOM versus included angles ranging from 0° to 60° and number of measurements ranging from 3 to 101. Also shown in the graph is a FOM plane which

equals one. All points on the graph above this plane were for cases in which the triangulation algorithm had a smaller error, while all points below this plane are for cases in which the angle-rate algorithm had better error performance.

From our analysis, we conclude that the angle-rate algorithm performs better than the standard triangulation algorithms once the number of measurements exceeds ten and the included angle is greater than 2°. On the other hand, when the included angle grows beyond 40°, the error using the angle-rate algorithm increases due to the tangent function producing significant approximation errors at these higher angles. The results show that the angle-rate emitter localization algorithm is a better choice over direct triangulation for small included angle AOA applications common to GDOP environments.

2) Kalman Filter Techniques: The primary purpose for using Kalman filtering techniques is to incorporate multiple sensor values of a stationary or moving target obtained over a time period, which is a problem significantly different from the triangulation and angle-rate algorithms we just presented. We envision that the Kalman filtering techniques, performed within one of the UAVs or at a ground unit, can be combined with one of the two aforementioned localization techniques to render better target localization accuracy.

Due to the capability of a Kalman filter to incorporate sensor measurements obtained from different perspectives and at different times, we demonstrate that a sensor measurement sequence and a sensor configuration have a direct impact on the ability to accurately locate a target.

We performed experiments each with a total of 100 available observations and up to ten different UAVs orbiting around the initial estimated position of a target. The choice of 100 total measurements ensures that the filter has sufficient iterations to converge. We varied three primary variables to explore the performance of the Kalman filtering approach in 12 different cases. The primary variables were as follows: 1) the type of sensors available on each UAV; 2) the configuration or spacing of the sensors in the orbit around a target; and 3) the scheduling sequence or order in which each UAV collects data on the target's location for the Kalman filter.

For the first variable, type of sensors, there were three different options for the UAVs: 1) All UAVs have the same low-quality sensors (noise covariances of 0.13 along range and 0.65 cross-range); 2) all UAVs have the same high-quality sensors (noise covariances of 0.1 along range and 0.5 cross-range); or 3) a mix of low- and high-quality sensors randomly distributed among UAVs, with an equal probability of each type of sensor to be chosen. Note that both sensor types possess Gaussian asymmetrical error distributions, as is characteristic of most airborne localization sensors.

The second primary variable, which is the configuration of the sensors in the search orbit, took one of two possibilities. The sensors were either uniformly distributed in a formation spanning the 360° of the orbit, which we refer to as a full orbit configuration, or they were uniformly distributed around 180° of the orbit, similarly referred to as a half orbit configuration. The second option may offer some advantages over the first by eliminating redundant measurements when two sensors are directly opposite of each other in orbit about a target.

The third primary variable was the scheduling sequence with two possible variations: 1) The sensor observations could be scheduled in order as one moves through the search orbit, so that adjacent sensors make observations in sequence, and 2) the sensors could be scheduled randomly among all available sensors.

With three sensor options, two configuration options, and two scheduling options, there were a total of 12 different cases to explore through simulation. For each of the 12 cases, we also varied the number of sensors involved in the search from one to ten, generating a total of 120 scenarios, each conducted 500 times to provide statistically sound mean estimates. For each simulation, the number of sensors observing a target remained constant, even though in an actual situation, the number would vary as UAVs join and depart a group involved in the orbit during the localization period. Note that, regardless of the number of sensors available for each scenario, the Kalman filter had access to a total of 100 observations during the simulation. Certainly, the number of observations increases in a given time with more UAVs if each UAV's sensing period is equal; however, the primary goal is not to compare the performance over time but over an equal number of observations as we vary the sensor configuration. Moreover, by the end of all simulations, the Kalman gain of the filter had already converged to a very small number, making the impact of any additional measurements negligible. Ultimately, we seek to investigate whether a set of inferior sensors configured and scheduled appropriately can outperform a set of sophisticated sensors if the total number of sensor readings is fixed in locating a target using Kalman filter estimation techniques. Results for the study of the impact of additional sensors over a fixed time window can be found in [23].

Fig. 9 shows the simulation results. Each frame within Fig. 9 contains three lines representing the different sensor options (all high-quality, all low-quality, and a random mix of high- and low-quality sensors). The standard deviations of the plotted means were less than 0.59 for sets of good sensors, less than 0.44 for sets of bad sensors, and less than 0.60 for mixed sets. The results shown in the figure should be viewed as follows. To see the effects of the UAV configurations on the localization performance as we add more UAVs to locate a target, observe how the cost varies along the x-axis for each frame. The cost is defined as the sum of the corresponding covariance matrix trace values across all filter updates from the 100 sensor measurements. To compare the performance of sensor positions that are equally distributed around the entire orbiting circle versus only the half of the orbiting circle, compare the same line (solid, dash–dotted, and dotted) between two vertically adjacent frames, such as frames (a) and (c). To see how different scheduling schemes affect the overall target localization performance, compare each line (solid, dash–dotted, and dotted) between two horizontally distributed frames, such as frames (c) and (d).

In all cases, introducing high-quality sensors into the localization problem reduced the total cost, as expected, which indicates that the Kalman filter produced a more accurate estimate of the target's location. However, note that, with effective sensing schedules, even if (solid lines) all bad sensors

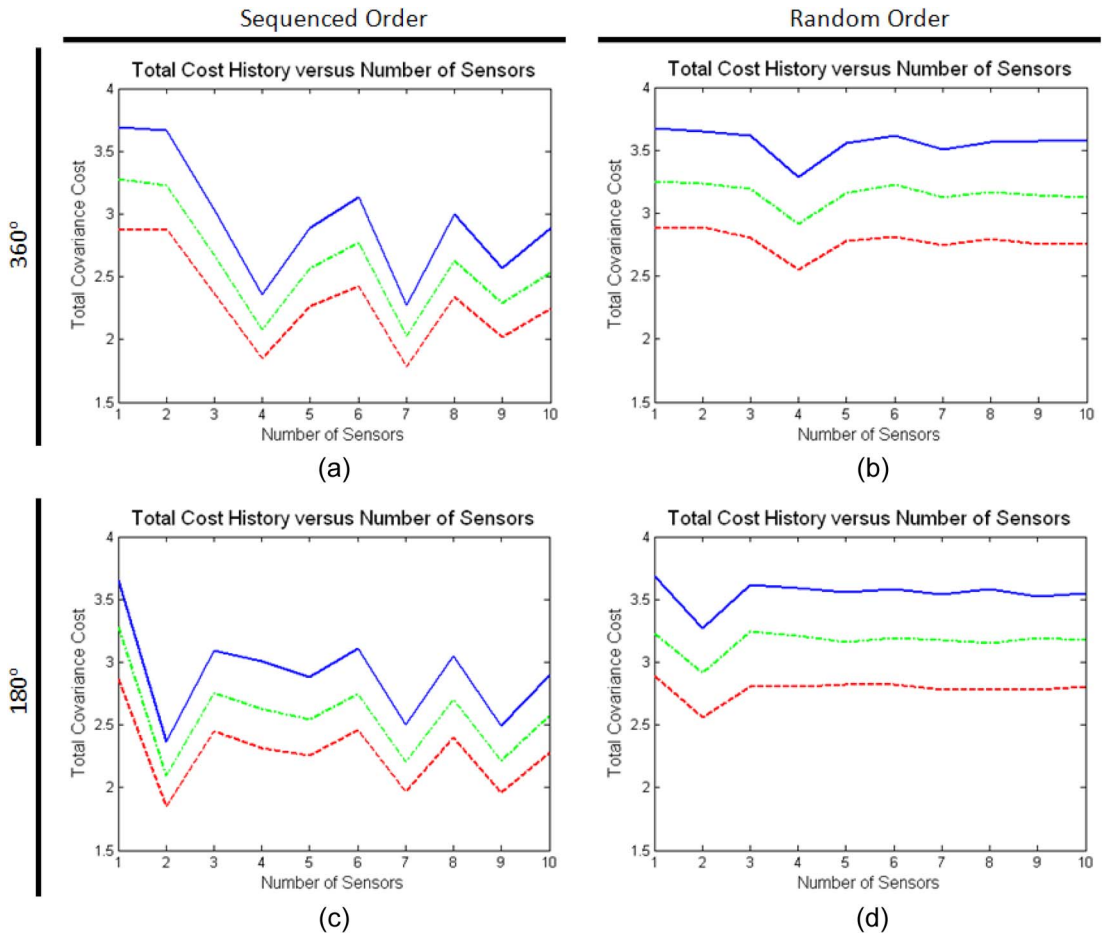

Fig. 9. Simulation results plotting the total covariance cost versus the number of sensors. The displayed mean values are the results of 500 simulations each. The solid lines represent simulations with only low-quality sensors, the dashed lines represent simulations with only high-quality sensors, and the dash–dotted lines represent simulations with a mix of high- and low-quality sensors with an equal probability of each sensor type. Cases (a) and (b) position the UAV sensors uniformly about a 360° orbit around the target's estimated position. Cases (c) and (d) position the UAV sensors uniformly about a 180° half orbit centered on the target's estimated position. Cases (a) and (c) use a sequenced scheduling where the UAVs observe the target in order as you move around the orbit. Cases (b) and (d) use a random scheduling where the next observation is selected at random from the available positions.

or (dash–dotted lines) a mixture of bad and good sensors are used, they can outperform the results obtained by using exclusively (dashed lines) good sensors. For example, consider the final localization accuracy values when seven UAVs are deployed in frames (a) and (b). The cost of the sequential order with bad sensors (2.36) outperforms that of the random order results with good sensors and a mixture of bad and good sensors (2.55 and 2.92, respectively). Certainly, if the bad sensors were to have been chosen to have an even greater uncertainty, at a certain point, the change in the ordering of the data would not have made them the most desirable choice, but even then, the choice of the sequencing pattern would still have a measurable impact on the filter's efficiency.

In addition to showing that it is possible to achieve better results with relatively bad sensors over those obtained using good sensors in suboptimal configurations, three additional conclusions can be drawn. First, the order of sensing a target is important. Given the same number of sensors, the sensor locations, the type of sensors, and the number of sensor readings, the sensor schedule, which is a factor that can typically be easily controlled, plays a significant role in the final outcome of the target location error. One can see this by picking a number of sensors in paired frames (a) and (b), or (c) and (d) and comparing the final accumulated location errors. For example, if one compares the dash–dotted lines (representing the use of low- and high-quality sensors) when only three sensors are used in a 180° configuration, the sequential and random orders produce final costs of 2.75 and 3.24, respectively, which is a significant $(\alpha = 0.01)$ difference that addresses the need for a "smart" sensor scheduling. Second, the sensor configuration is important. Again, given the same number of sensors, the type of sensors, the number of sensor readings, and the sensor schedule, the placement of sensors has direct impact on the final target localization result. One can observe this point by comparing frames (a) and (c). Suppose you have only two sensors at your disposal, the solid lines (representing the use of low-quality sensors only) in frames (a) and (c) show the final target location error values of approximately 3.66 and 2.37, respectively. Physically, in this case, it means that its better to place two sensors at a 90° angle rather than placing them facing each other. Finally, a higher number of sensors without considering the sensor schedule and configuration do not translate to a better target localization performance. One can see this last finding by comparing the final cost values within

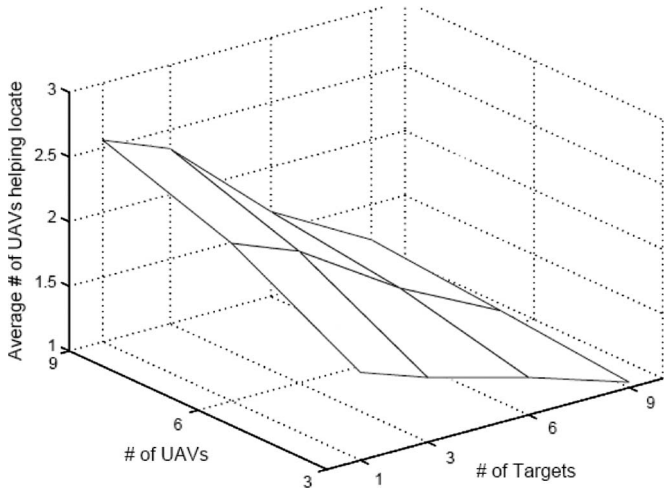

Fig. 10. Plot of the average number of UAVs cooperating for each localization estimate when the number of UAVs changes from three to nine and the number of targets changes from one to nine.

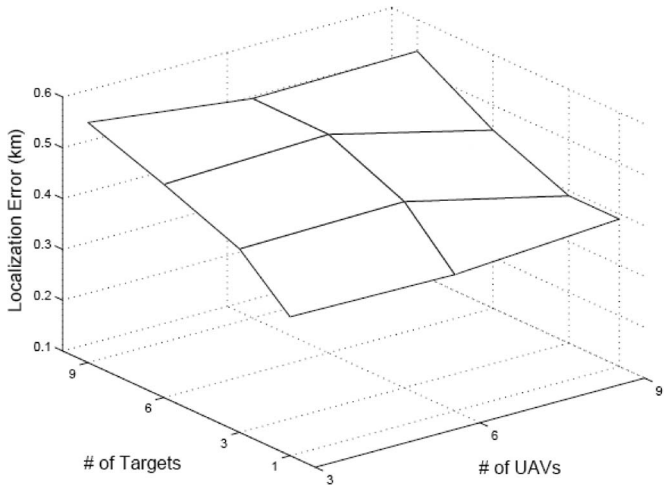

Fig. 12. Plot of the average localization error in kilometers when the number of UAVs changes from three to nine and the number of targets changes from one to nine using a 7° accurate sensor.

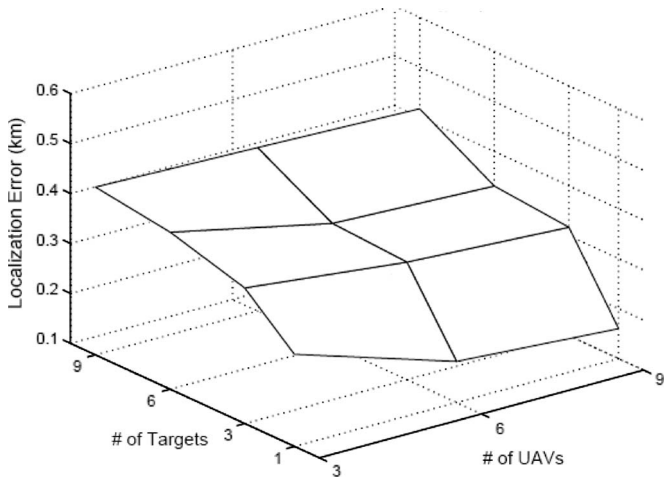

Fig. 11. Plot of the average localization error in kilometers when the number of UAVs changes from three to nine and the number of targets change from one to nine using a 1° accurate sensor.

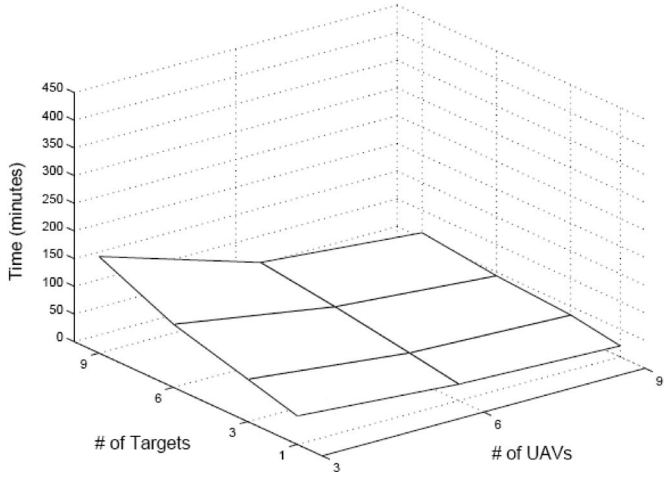

Fig. 13. Plot of the average total search/localization time in minutes when searching a 50 × 75 km area as the number of UAVs changes from three to nine, and the number of targets changes from one to nine.

each frame or across multiple frames. For example, consider the dashed line in frame (a). Clearly, the performance increases up to four sensors (cost of 1.85) but does not get any better as one adds additional sensors until one reaches a second minimum at seven sensors (cost of 1.78).

C. Search and Localization Joint Performance

In this section, we present the overall performance of multiple UAVs as we vary the ratio of the number of UAVs to the number of targets. One hundred simulation runs were conducted for each combination of three, six, or nine UAVs, and one, three, six, or nine targets. The initial target and UAV locations were randomly selected in a 50 km × 75 km area. The UAVs flew in a velocity range between 115 and 260 km/h (cruise at 115 km/h) with a minimum turn radius of 0.5 km. The targets traveled in random directions for random distances with a maximum velocity of 38 km/h. The targets emitted signals randomly for an average of 6.8 min and were silent for an average of 4.8 min. The sensor mounted on the UAVs provided AOA estimates every 12 s. For the sake of comparison, we ran simulations using sets of directional sensors with 1° and 7° accuracy. The maximum sensor range was assumed to be 4.3 km, and during LT, the UAVs flew at an orbit of 2.2 km from the estimated target location. The triangulation technique discussed in Section IV was used, with the localization process for a specific target continuing until the target stopped emitting. Since the emitters can turn off at any moment, quite often, the ideal number of UAVs and proper geometry was not achieved before the localization estimate was finalized.

Fig. 10 shows the tradeoff between the number of UAVs operating in the cooperative target localization stage and the overall GS. As expected, the best localization cooperation (more than 2.5 UAVs per localization effort) was achieved when nine UAVs faced only one target, while the cooperation reduced as the ratio changed down to three UAVs versus nine targets. The amount of cooperation had a positive impact on the localization accuracy, as seen in Figs. 11 and 12. For the sensor with 1° accuracy, the average error for three UAVs versus nine targets

was greater than 0.4 km, and the error was reduced to 0.16 km when nine UAVs are used to locate one target. For the sensor with 7° accuracy, with three UAVs locating nine targets, the average error was 0.57 km, while the average error was reduced to 0.38 km with nine UAVs locating one target. Fig. 13 shows the total time spent on search and localization. As expected, the best time (19 min) occurred when nine UAVs faced only one target; the time increased up to 174 min when three UAVs faced nine targets.

VI. Conclusion

In this paper, we introduced a novel decentralized cooperative control architecture for the tasks of searching, detecting, and localizing mobile ground targets intermittently emitting RF signals, where each UAV determines its actions based on its sensor information and the data shared among neighboring UAVs. Particular focus was given to the proposed search strategy that was demonstrated to generate efficient cooperative search patterns based exclusively on a search cost computed by each UAV. The beneficial impact of each element of the search cost function toward the overall collective goals was demonstrated with proof-of-concept simulations.

To deal with mobile ground targets that intermittently emit signals, a special focus was also given to the localization techniques to efficiently integrate the information of multiple AOA sensors over time. In particular, we compared the localization outcomes when we applied triangulation, the angle-rate algorithm, and Kalman filtering techniques. The angle-rate algorithm was shown to be more suited than the triangulation method for the small included angle cases common to target localization from a single UAV orbiting an emitter. With the tradeoff of additional computational requirements, Kalman filtering, which, in addition to position estimation, provides covariance estimation, was further investigated with simulation results demonstrating the effects of sensor locations, types, and scheduling techniques. The results of the investigation indicate that a structured scheduling approach can improve the quality of the target position estimates. When comparing the localization performance based on the overall configuration options, we found that orthogonal positioning of the sensors on a half orbit produced optimal results. Work is currently underway on an approach that combines elements of the three techniques to generate a localization technique that is accurate and robust in all circumstances.

Finally, we presented results demonstrating the cooperative search and localization capabilities of multiple UAVs and targets. With detailed results published in [24], we have successfully applied the conclusions reached in this paper to hardware flight tests involving UAV platforms.

References

[1] S. Saripalli, D. J. Naffin, and G. S. Sukhatme, "Autonomous flying vehicle research at the University of Southern California," in *Proc. Int. Workshop Multi-Robot Syst.*, 2002, pp. 73–82.

[2] J. J. Enright and E. Frazzoli, "UAV routing in a stochastic, time-varying environment," in *Proc. IFAC World Congr.*, Prague, Czech Republic, 2005.

[3] W. Jizhou, L. Zongjian, and L. Chengming, "Reconstruction of buildings from a single UAV image," in *Proc. Int. Soc. Photogramm. Remote Sens. Congr.*, Istanbul, Turkey, 2004, pp. 100–103.

[4] J. Everaerts, N. Lewyckyj, and D. Fransaer, "PEGASUS: Design of a stratospheric long endurance UAV system for remote sensing," in *Proc. Int. Soc. Photogramm. Remote Sens. Congr.*, Istanbul, Turkey, 2004, pp. 29–33.

[5] F. Bourgault, T. Furukawa, and H. T. Durrant-Whyte, "Coordinated decentralized search for a lost target in a Bayesian world," in *Proc. IEEE/RJS Conf. Intell. Robot. Syst.*, Las Vegas, NV, Oct. 2003, pp. 48–53.

[6] L. Parker and B. Emmons, "Cooperative multi-robot observation of multiple moving targets," in *Proc. Int. Conf. Robot. Autom.*, Albuquerque, NM, Apr. 1997, pp. 2082–2089.

[7] N. Miyata, J. Ota, T. Arai, and H. Asama, "Cooperative transport by multiple mobile robots in unknown static environments associated with real-time task assignment," *IEEE Trans. Robot. Autom.*, vol. 18, no. 5, pp. 769–780, Oct. 2002.

[8] T. Simeon, S. Leroy, and J. Laumond, "Path coordination for multiple mobile robots: A resolution-complete algorithm," *IEEE Trans. Robot. Autom.*, vol. 18, no. 1, pp. 42–49, Feb. 2002.

[9] L. Van Breda, "Operator performance in multi Maritime Unmanned Air Vehicle control," TNO Human Factors Res. Inst., Soesterberg, The Netherlands, Rep. TNO-TM 1995 A-76, 1995.

[10] P. Vincent and I. Rubin, "A framework and analysis for cooperative search using UAV swarms," in *Proc. ACM Symp. Appl. Comput.*, 2004, pp. 79–84.

[11] P. DeLima, D. Pack, and J. C. Sciortino, Jr., "Optimizing a search strategy for multiple mobile agents," in *Proc. Conf. Int. Soc. Opt. Eng.*, 2007, vol. 6563, p. 656 30B.

[12] W. Burgard, M. Moors, D. Fox, R. Simmons, and S. Thrun, "Collaborative multi-robot exploration," in *Proc. Int. Conf. Robot. Autom.*, 2000, pp. 476–481.

[13] G. York and D. Pack, "Comparative study on time-varying target localization methods using multiple unmanned aerial vehicles: Kalman estimation and triangulation techniques," in *Proc. IEEE Int. Conf. Netw., Sens., Control*, Tucson, AZ, Mar. 2005, pp. 305–310.

[14] H. Gilbert, J. McGuirk, and D. Pack, "A comparative study of target localization methods for large GDOP," in *Cooperative Systems: Control and Optimization*, vol. 588, D. Grundel, R. Murphey, P. Pardalos, and O. Prokopyev, Eds. Berlin, Germany: Springer-Verlag, 2007.

[15] R. E. Kalman, "A new approach to linear filtering and prediction problems," *J. Basic Eng.*, vol. 32, pp. 35–45, 1960.

[16] E. Nettleton, M. Ridley, S. Sukkarieh, A. Goktogan, and H. Durrant-Whyte, "Implementation of a decentralized sensing network aboard multiple UAVs," *Telecommun. Syst.*, vol. 26, no. 2–4, pp. 256–284, Jun. 2004.

[17] D. Pack and B. Mullins, "Toward finding a universal search algorithm for swarm robots," in *Proc. IEEE/RJS Conf. Intell. Robot. Syst.*, Las Vegas, NV, Oct. 2003, pp. 1945–1950.

[18] D. Pack and G. York, "Developing a control architecture for multiple unmanned aerial vehicles to search and localize RF time-varying mobile targets: Part I," in *Proc. IEEE Int. Conf. Robot. Autom.*, Barcelona, Spain, Apr. 2005, pp. 3965–3970.

[19] K. Morris, B. Mullins, D. Pack, and R. Baldwin, "Impact of limited communications on a cooperative search algorithm for multiple UAVs," in *Proc. IEEE Int. Conf. Netw., Sens., Control*, Ft. Lauradeal, FL, Apr. 2006, pp. 572–577.

[20] M. A. Batalin and G. S. Sukhatme, "Multi-robot dynamic coverage of a planar bounded environment," Robotic Embedded Systems Laboratory, Univ. Southern Calif., Los Angeles, CA, 2002. Tech. Rep.

[21] J. Ousingsawat and M. G. Earl, "Modified lawn-mower search pattern for areas comprised of weighted regions," in *Proc. Amer. Control Conf.*, Jul. 9–13, 2007, pp. 918–923.

[22] D. Pack, G. York, and R. Fierro, "Information-based cooperative control for multiple unmanned aerial vehicles," in *Proc. IEEE Int. Conf. Netw., Sens., Control*, Ft. Lauderdale, FL, Apr. 2006, pp. 672–676.

[23] G. J. Toussaint, P. DeLima, and D. Pack, "Localizing RF targets with cooperative unmanned aerial vehicles," in *Proc. Amer. Control Conf.*, Jul. 2007, pp. 5928–5933.

[24] Y. Yoon, S. Gruber, L. Krakow, and D. Pack, "Autonomous target detection and localization using cooperative unmanned aerial vehicles," in *Proc. Int. Conf. Cooperative Control Optimization*, Jan. 2008, pp. 195–206.

Daniel J. Pack (S'91–M'95–SM'02) received the B.S. degree in electrical engineering from the Arizona State University, Tempe, in 1988, the M.S. degree in engineering sciences from Harvard University, Cambridge, MA, in 1990, and the Ph.D. degree in electrical engineering from Purdue University, West Lafayette, IN, in 1995.

He is a Professor with the Department of Electrical and Computer Engineering, U.S. Air Force Academy, Colorado Springs, CO. He has coauthored three textbooks on embedded systems and published over 70 refereed journal and conference papers on control, robotics, pattern recognition, and engineering education. His research interests include unmanned aerial vehicles, intelligent control, automatic target recognition, and robotics.

Dr. Pack is a member of Eta Kappa Nu, Tau Beta Pi, and the American Society for Engineering Education. He is a registered Professional Engineer in Colorado. He has received a number of teaching and research awards, including the Carnegie Foundation's Colorado Professor of the Year Award, the Tau Beta Pi Professor of the Year Award, the Outstanding Academy Educator Award, and the Seiler Award in Research Excellence.

Pedro DeLima received the B.S. degree in electrical engineering with emphasis in automation and control from the University of São Paulo, São Paulo, Brazil, in 2000 and the Ph.D. degree in electrical engineering from Oklahoma State University, Stillwater, in 2005.

He was an Instructor with Oklahoma State University in 2005, while giving continuity to his research in adaptive critic architectures, neural networks, automated decision logics, and genetic algorithms with applications to fault-tolerant control and temporal fuzzy modeling. He is currently a Research Associate with the U.S. Air Force Academy, where his work focuses on the development of decentralized cooperative strategies for multiple unmanned aerial vehicles for search, detection, and localization subject to real-world dynamics and communication restrictions.

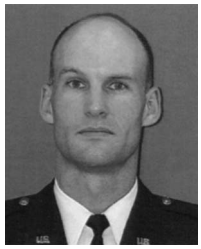

Gregory J. Toussaint (SM'06) received the B.S. degree in electrical engineering from Cornell University, Ithaca, NY, the M.S. degree in systems engineering from the Air Force Institute of Technology, Wright-Patterson Air Force Base, OH, and the Ph.D. degree in electrical engineering from the University of Illinois, Urbana, where he studied control theory applied to nonlinear systems.

He is the Deputy Department Head and an Assistant Professor with the Department of Electrical and Computer Engineering, U.S. Air Force Academy, Colorado Springs, CO. As an active duty Air Force officer, he has also held assignments with the Air Force Research Laboratories as a Program Manager in a system program office and as a Branch Chief at an intelligence center.

George York received the B.S.E.E. degree from the U.S. Air Force Academy, Colorado Springs, CO, and the M.S.E.E. and Ph.D. degrees in electrical engineering from the University of Washington, Seattle.

He is the Program Manager with the Air Force Office of Scientific Research, London, U.K. He supports research in sensors, antennas, signal processing, RF weapons, superconductivity, and space weather. He manages over 50 programs in 28 countries throughout Europe, Africa, and the former Soviet Union. Previously, he was an Associate Professor with the U.S. Air Force Academy, where he was a member of the Unmanned Aerial Vehicle (UAV) Research Group, developing algorithms to cooperatively control multiple UAVs. His principal fields of interest are sensor networks, embedded computing, signal processing, medical ultrasound, and engineering education. He has authored more than 40 publications and inventions in these areas.